Tunable spatial heterodyne spectroscopy (TSHS): a new technique for broadband visible interferometry

S. Sona Hosseini[a], Aaron Gong[a], Dustin Ruth[a], Hector A. Baldis[a], Walter Harris[a]

[a]UC Davis, Applied Science, Engineering III, One Sheilds Ave., Davis, CA, USA 95616

ABSTRACT

In the study of faint, extended sources at high resolving power, interferometry offers significant etendue advantages relative to conventional dispersive grating spectrometers. A Spatial Heterodyne Spectrometer (SHS) is a compact format two-beam interferometer that produces wavenumber dependent 2-D Fizeau fringe pattern from which an input spectrum can be obtained via a Fourier transform. The sampled bandpass of SHS is limited by the highest spatial frequency that can be sampled by the detector, which is typically less than 10 nm. This limitation has made these instruments useful primarily for studies of single emission line features or molecular bands. To date there have been few broadband implementations. We describe here continuing progress toward development of a broadband tunable SHS (TSHS) that is based on an all-reflective format where a single grating operates simultaneously as a beam-splitter, dispersive element, and beam combiner. The narrow spectral coverage of the TSHS is moved to different tuning wavenumbers by adjusting the angle of the pilot mirrors that guide the interfering beams through the optical path, thus slewing the acceptance band over a much broader spectral range. Our present effort involves a breadboard laboratory prototype of a second-generation TSHS in which we address several technical limitations of an earlier version. In particular the new design reduces wavefront distortions on the pilot mirrors, solves problems with magnification and focus of the fringe localization plane onto the detector, and addresses the variability in sensitivity and resolving power limitations of using a single grating over a large bandpass.

Keywords: Spectroscopy, Interferometry, SHS, Faint diffuse sources, Ultraviolet, Remote sensing

1. INTRODUCTION

The purpose of this paper is to discuss the methodology and need for new technology in broadband high-resolution spectroscopy based on the emerging technique of spatial heterodyne spectroscopy. High-resolution spectra carry more information than low-resolution spectra, but it is the cost of that added information that must be weighed against other factors. Observations of the intensity and line profile of emission and absorption lines have become a staple technique for the study of astronomical targets. However, the requirements for wavelength range and resolution differ depending on the characteristics of the source. In the solar system, diagnostic emission line sources (e.g., interplanetary medium, comets, planetary upper atmospheres, and planet and satellite near space environments) are typically faint, buried under the reflected continuum of the Sun and angularly extended from a remote sensing perspective. Basic parameters like composition, distribution, intensity and energy distribution can be studied with low-resolution spectroscopy. High-resolution spectroscopy can reveal additional information about the physical characteristics of a source such as velocity, temperature, pressure, isotopic signatures, etc. The range of temperatures and velocities experienced in Solar System targets are usually small ($V \leq 50$km/sec and $T < 1000$K), and they therefore require high resolving power (R) by comparison with stellar and galactic sources with very high temperatures and velocities. Unfortunately, this also means that the standard for high resolving power at many ground-based telescopes ($R \sim 15000$) is still relatively low for planetary science. In the case of space based remote probes, there is an almost complete lack of high resolving power instruments that operate in the UV-Visible range [1,2].

There are several instrumental methods to obtain high resolving power spectra. The most common is the classical grating spectrometer, but their high resolving power implementations are physically very large and require large aperture telescopes to overcome the small angular size of the apertures required. This makes them incompatible with the volume and mass restrictions of space probes. Interferometry (e.g., Scanning Fourier Transform Spectrometers-FTS, Fabry-Perot Interferometers-FPI) is another method that is frequently used to obtain high étendue measurements at high R and can be compact enough for space use [3]. However, these instruments tend to have progressively more challenging optical tolerance issues at shorter Visible and UV wavelengths [4] or rely on transmitting optics that set a lower limit on the wavelength range where they can be used. Transmission begins to become problematic below 3000Å where many commercially available glasses begin to become opaque. In the vacuum UV, especially below 1600Å, the number of transmitting crystals is sharply reduced and the performances of those that remain begin to degrade. The last known transmitter, LiF, becomes opaque at ~1050Å, and is difficult to make optically flat for a beam splitter or etalon. Getting spectra below 1000Å requires mirrors coated with Boron-Carbide or Silicon-Carbide (≤35% reflectivity) or multi-layer coatings that act like narrow band filters. This is unfortunate, because the UV is rich territory for solar system study; the solar continuum intensity drops rapidly for $\lambda<4000$Å, and the emission lines below 1500Å completely dominate the Sun's spectrum. This allows relatively uncontaminated access to auroral and other atmospheric emissions. Therefore, the most efficient way to gain access to this spectral information is to use all reflective instruments [1,4].

An emerging technology that addresses all mentioned problems is SHS. The development of SHS has opened a middle ground of providing a combination of small bandpass and high resolving power (R~50000–100000) over a large field of view (FOV). SHS systems are compact, lightweight, and can be constructed with no moving parts at all or only a single rotation mechanism. The optical tolerances of SHS, both for the surface flatness of the components and the precision of their placement, are substantially relaxed compared to other interferometric techniques. This makes SHS easier to align at shorter wavelengths and less sensitive to thermo-mechanical drift in the optical components. This has led to their increasing use for ground spaced based UV-Visible applications [5,6,7,8]. This combination makes them ideal candidates for space missions and ground-based observations of extended targets as either as stand-alone instruments or at the focus of small to intermediate aperture telescopes. A major drawback to the SHS technique is that its basic design is limited to a very narrow bandpass around a single target wavelength.

In this paper, we provide a detailed description of the unique characteristics of the anti-aliased all-reflective tunable design SHS. We compare some of the mathematical differences between the reflective and more common Michelson-style SHS designs and summarize progress toward the development of a second-generation tunable form of the SHS that builds on previous work.

2. ALL REFLECTIVE TUNABLE SHS

2.1 Mathematical concepts, and Fringe pattern

Scientific SHS instruments were first developed by Roesler and Harlander [9]. They added the idea of using a two-dimensional light-sensing array at the instrument focal plane to the previous related work by Connes and Dohi and Susuki [10,11]. Their SHS configuration was a Michelson-style interferometer in which the mirror in each interferometer arm has been replaced by a grating rotated to the first order Littrow configuration for a single wavelength producing 2 dimensional fringe pattern with the spatial intensity frequency, in 1 dimension, of

$$f_x = 4(\sigma - \sigma_0)\tan\beta_L \ , \qquad (1)$$

where β_L is the Littrow angle, σ is the wavenumber, and σ_0 is the Littrow wavenumber. For a polychromatic source, the fringe intensity pattern is given by

$$I(x) = \int_0^\infty S(\sigma)(1 + \cos 2\pi f_x x)d\sigma \quad , \qquad (2)$$

where x is the location on the fringe localization plane (FLP) and $S(\sigma)$ is the input spectrum. There are several excellent mathematical treatments of this style of SHS in the literature to which the interested reader is referred [1,2,9,12,13].

As mentioned in section 1, effective use of the SHS technique in vacuum UV to extreme UV range requires abandoning transmitting optics and instead using an all-reflective system. All-reflective SHS systems were first proposed by Roesler and Harlander [9] and were later developed and successfully used for ground [8,14], and space applications [7,8]. The reflective SHS design is mathematically distinct from the refractive version, but, as we show below, converges to a very similar set of performance characteristics in the limit of small angles.

The all-reflective SHS is a common-path interferometer. It splits the incoming light beam into two beams, both of which pass through the same path before exiting the interferometer. A symmetrically ruled grating acts as both a beam-splitter and as a dispersing element that splits the incoming collimated light into ±m orders with same efficiencies at an angle θ that is defined by the groove shape and wavelength.

In the all-reflective SHS shown in figure1, collimated light enters the interferometer, is incident on the grating with angle β_{in1}, and is split symmetrically, by dispersion, into the ± m orders at angles ± β_{out1} with respect to the normal. The beams circulate in opposite directions; reflecting off the two flat mirrors, return to the grating at an angle $\beta_{in2,}$ a distance ±h from their first incident point on the grating, perpendicular to the grooving axis. Order m= +1 and m= −1 will have the same absolute separation |h| distance, but impact the grating on opposite sides of the incident point of the incoming beam, along the x axis. As will be shown, the distance 'h' also depends on all the incoming angles parameters and the SHS setup parameters. The beams diffract for second time into an angle β_{out2}, and then exit the interferometer. The interference in this configuration results purely from an angular divergence between the two exiting wavevectors, because, due to the symmetry, there is no optical path difference between the two beams.

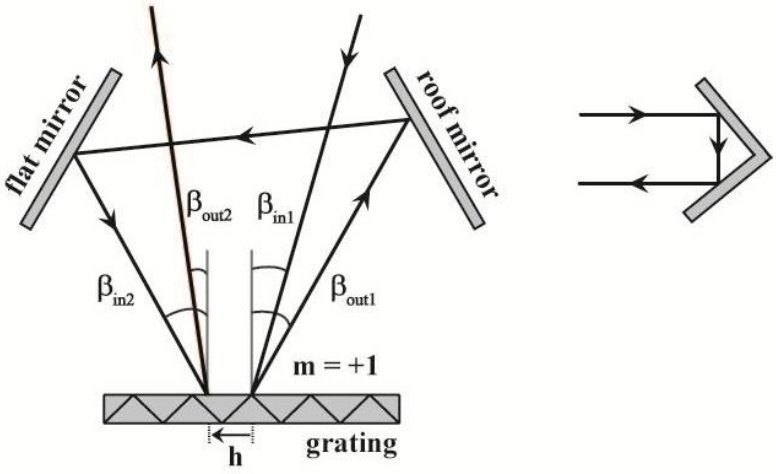

Figure 1. The optical path of light beam inside SHS. For clarity only m= +1 order is shown and the first diffraction and the angles and distances are exaggerated. The roof mirror is substitute for one of the flat mirrors to translate the beam off the plane of interference.

One apparent problem with all-reflective SHS design is that if we use two plane flat mirrors, the incoming and outgoing beams then overlap. One design proposed by Harlander et al. [9] overcame this problem by adjusting the angle of the flat mirrors so that the returning beams meet at a point offset in the dispersion plane from the incoming location. This approach was successfully used by Chakrabarti, et al. [7] for a sounding rocket experiment. Although it conserves the

minimum two reflections, this design loses the line of symmetry where all wavefronts interfere positively. In our design, we are using the roof mirror translation [9,15] that permits us to center the incoming and outgoing beams at the same horizontal (dispersion plane) location on the grating. The output interferogram will then have zero-path difference at the center of the grating, and the input and output beams are on the same axis of symmetry such that the central band of positive interference is retained. The most significant disadvantage of the roof mirror SHS is from losses due to the additional reflection in the roof. These losses are negligible (<10%) until well into the vacuum UV (VUV), but increase rapidly with decreasing wavelength thereafter. In the extreme UV, single reflection losses can exceed 65% [15] unless special multi-layer coatings are used.

For a single wavelength everything is symmetric in the sense that $\beta_{in1}= \beta_{out2}$; This wavelength is called the 'heterodyne wavelength'. In this case, the exiting wavevectors will emerge in phase, with their wavefronts parallel following a path identical to the incoming beam; therefore, they interfere positively everywhere and as it is shown in figure2, there is no interference pattern for the heterodyne wavelength.

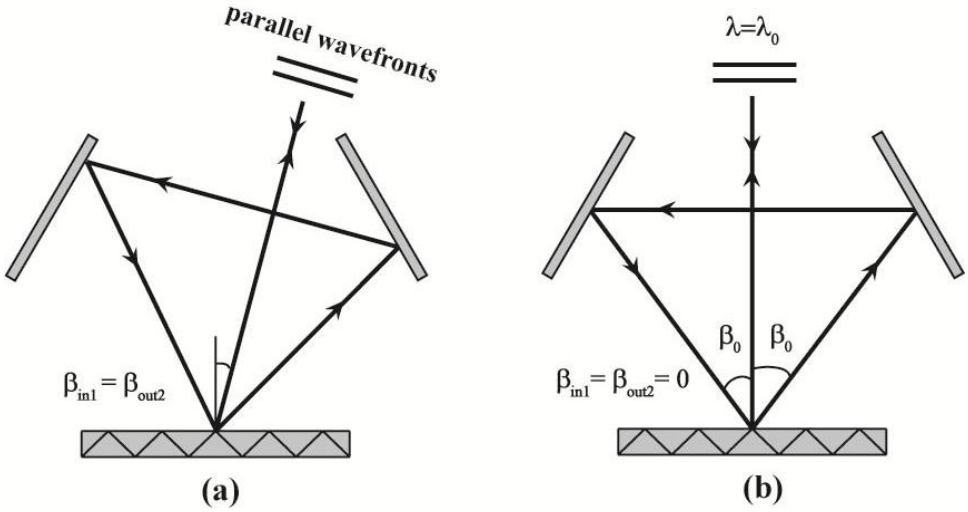

Figure 2. (a) The general condition for the heterodyned wavelength is when h= 0 and $\beta_{in1}=\beta_{out2}$. (b) The heterodyne wavelength that is incident on the grating by $\beta_{in1}= 0$ is called λ_0, in which it will have $\beta_{out1}=\beta_0$, $\beta_{in2}=\beta_0$, $\beta_{out2}= 0$.

In the general case of an extended source and a wavelength not aligned to the zero path geometry, there are different cases for the incoming light. Figure 3 shows that the incoming light that is incident on the grating can be considered to come from the corners of a pyramid. The variations in β_{in1} can take place in two dimensions: either perpendicular to groove axis in xz plane, defined by α, or along the groove axis in yz plane, defined by α'. The variations for light entering the SHS at a wavelength other than λ_o are specified by $\Delta\lambda$. The most general incoming beam is defined by extremes in β_{in1} and wavelength λ that are $\beta_{in1}=\alpha+\alpha'$ and $\lambda=\lambda_0+\Delta\lambda$. In each case we can find all the characteristic angles of the beams by using the grating equation. The grating equation is:

$$[\sin\beta_{in} + \sin\beta_{out}] \cos\Phi = mG\lambda \qquad (3)$$

where β_{in} is the incoming beam angle in the diffraction plane, β_{out} is the diffracted angle, Φ is the angle between the incoming beam plane and the grating diffraction plane, G is the groove density in number of grooves per mm, m is the order of the diffraction, and λ is the wavelength. In figure 3, the xz plane is the plane of dispersion and interference. Therefore α will contribute to the incoming angle (β_{in}) in the grating equation and α' will contribute in the Φ term.

In this paper, the heterodyne wavelength at normal incidence ($\beta_{in1}=0$) is defined by λ_0. For λ_0, $\beta_{out1}=\beta_0$, and $\alpha=\alpha'=0$ (figure 2, right). All other incoming beam cases are compared to this case. The most general incoming beam is when $\beta_{in1}=\alpha+\alpha'$, $\lambda=\lambda_0+\Delta\lambda$, in which the $\beta_{out1}=\beta_0+\Delta\beta_{\alpha\alpha'\lambda}=\beta_0+\Delta\bar{\beta}$. Solving for this case, allows any angle or wavelength offset to be inserted and to obtain the output for all locations in the field of view.

There is degeneracy between the incoming beam cases and the *apparent* wavelength from the perspective of the interferometer. Grating equation shows that $\Delta\lambda$ and α (in the limit of small angles) have nearly identical effects on the output angle β_{out2}. Indeed, from the perspective of fringe frequency, it is not possible to determine which is acting. The coupling between $\Delta\lambda$ and α' is less direct, and the effect of α' on β_{out2} is much smaller than for α. This degeneracy is one of the main limiting factors for defining the R and FOV of SHS, because if α produces a change in $\Delta\lambda$ larger than the smallest resolvable wavelength element (i.e., the wavelength spacing between adjacent fringe frequencies), then the there is no apparent way to separate changes in incoming angle (FOV) from color in the power spectrum.

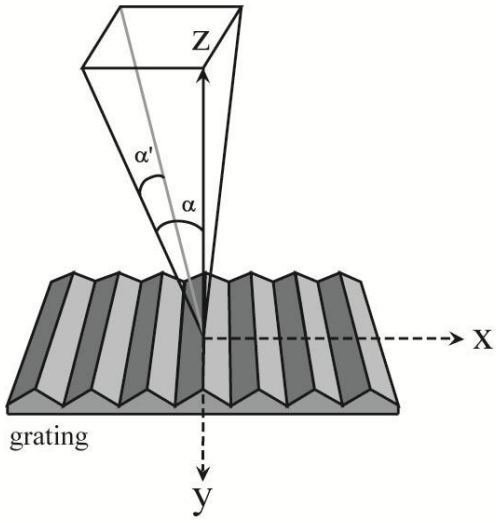

Figure 3. Incoming light is incident on the grating from the corners of a pyramid defined by the incoming angles α and α'. The z-axis is chosen to be on the optical path, the y axis along the groove density and the x axis is fixed by z and y axis.

The change in the first dispersion angle from β_0 results in a different path through the interferometer comparing to λ_0. It can be shown for the most general incoming beam, $\Delta\bar{\beta}$ is given by:

$$\Delta\bar{\beta} = \sin^{-1}\left\{\frac{\sin\beta_0+mG\Delta\lambda}{\cos\alpha'} - \sin\alpha\right\}. \quad (4)$$

The beam will be incident on the grating for second time with angle $\beta_{in2}=\beta_0-\Delta\bar{\beta}$ at the 'h' distance along x axis, given by:

$$h = L\cos\beta_0\left[\tan\beta_0 - \tan\left(\beta_0 - \Delta\bar{\beta}\right)\right], \quad (5)$$

where L is the average optical path inside SHS. The 'h' distance of the xz plane offset on the grating is perpendicular to the groove axis and symmetrically located on either side of the location of the original incident light for the two beams. The outgoing beam angles in this configuration can be shown to be:

$$\beta_{out\,2} = \sin^{-1}\left\{\frac{\sin\beta_0+mG\Delta\lambda}{\cos\alpha'} - \sin(\beta_0 - \Delta\bar{\beta})\right\}. \quad (6)$$

Everything is symmetric for both beams except that they pass through the SHS in opposite directions. In this case then, β_{out2} will be same in absolute magnitude for both beams; as a result, they will be diverging or converging simultaneously. The fringe intensity spatial frequencies in this case are

$$f_x = 2\sigma \sin\beta_{out\,2} \cos\alpha' \,, \qquad f_y = f_z = 0 \,, \tag{7}$$

where $\sigma = 1/\lambda$ and $\sigma_0 = 1/\lambda_0$. In this case, at the xy plane, the fringe pattern has intensity I(x) distribution given by equation(2).

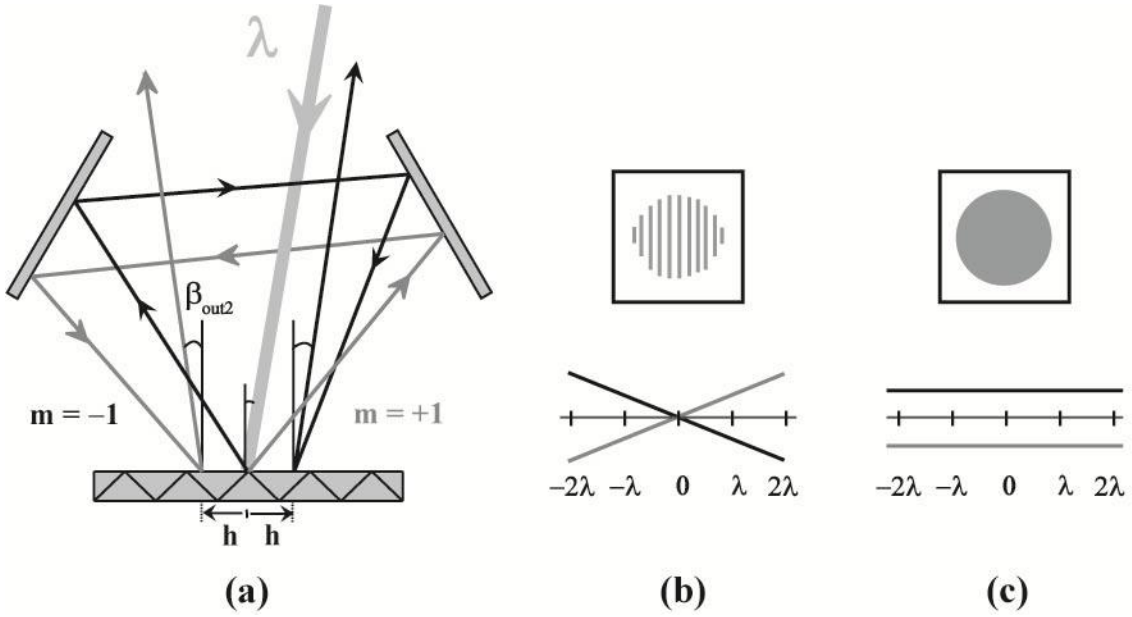

Figure 4. (a) The optical path through an all-reflective SHS for a non heterodyne wavelength. The general incoming beam is drawn as a wide bright beam. After the first incident on the grating, the incoming light diffracts into two symmetric orders, which are shown with black and gray colors. (b) For all other wavelengths than heterodyne wavelengths, the wavefronts will exit non-parallel and produce a fringe pattern. (c) In the symmetric case of the heterodyne wavelength, the wavefronts emerge parallel and in phase. Hence, they do not produce interference pattern. For clarity, the angles and the distances are exaggerated.

In all previous SHS literature the mathematical development for the Michelson design SHS was approached for normal incidence incoming light ($\alpha=\alpha'=0$) in the small angle approximation. For comparison with equation (1), the spatial fringe frequencies, in the small angle approximation for $\lambda=\lambda_0+\Delta\lambda$ and $\beta_{in1}=0$, in all reflective design is given by:

$$f_x = 4\,(\sigma - \sigma_0)\sin\beta_0 \,, \qquad f_y = f_z = 0 \,, \tag{8}$$

and the fringe intensity pattern is generated from equation (2). This result is the same fringe frequency that was reported by Chakrabarti et al. [7] for a non-symmetric all reflective SHS design and by Harlander for another all reflective SHS design [9].

For coherent collimated light from a point source (e.g., laser, star), the fringes form everywhere and therefore the fringe pattern can be said to be non-localized. However, for all other locations in the field of view, there is a region where the two extended beams have the highest overlap resulting in the highest fringe pattern contrast. While the center of the region is the same for all points in the field, as one moves from the center to the edge of the field of view, the confinement of this region increases until it approaches a plane. Therefore, if one expects to obtain the full field spectrum the output imaging optics must reimage the most restricted portion of this region onto a detector. This is referred to as the *fringe localization plane* (FLP), though it actually represents the region of best contrast with a maximal field of view contribution. Harlender [9] and Chakrabarti et. al., [7] have shown that the location of the fringe localization plane is a function of the path L and β_o and hence it moves significantly as a function of heterodyne wavelength.

The symmetry of the circulating all-reflective has the benefit of adding stability to the entire system. Any small movements in an optical component affect both interferometer arms almost equally, resulting in almost the same change in the path difference between recombining beams. The result is a system that, once aligned, is highly tolerant of thermo-mechanical drift. This is a key point in a comparison with FTS. Even small misalignment of the mirrors in a FTS system results in a loss of interference. By contrast, rather large changes can occur in mirror placement and alignment can occur in SHS without affecting interference at all. These changes affect only the heterodyne wavelength, which can be recovered by comparison with a test lamp spectrum. For SHS, the important quantity is tuning *stability* once a heterodyne wavelength is selected.

2.2 Fringe pattern in an anti-aliasing design

One of the major limitations of the single plane mirror is that the symmetry in achieved spectrum from the Fourier transform of the single plane mirror design duplicates all spectrum features at locations on either side of λ_0. In other words, there is no mechanism in the basic design to tell the difference between $\lambda_o+\Delta\lambda$ and $\lambda_o-\Delta\lambda$; both produce the same frequency and intensity distribution. This problem is referred to as *aliasing* and it can introduce insurmountable confusion in the inverted spectrum. This is acceptable when the spectrum consists of widely spaced lines with known rest wavelengths. However, for complex or continuum spectra, the resulting confusion renders the output unusable.

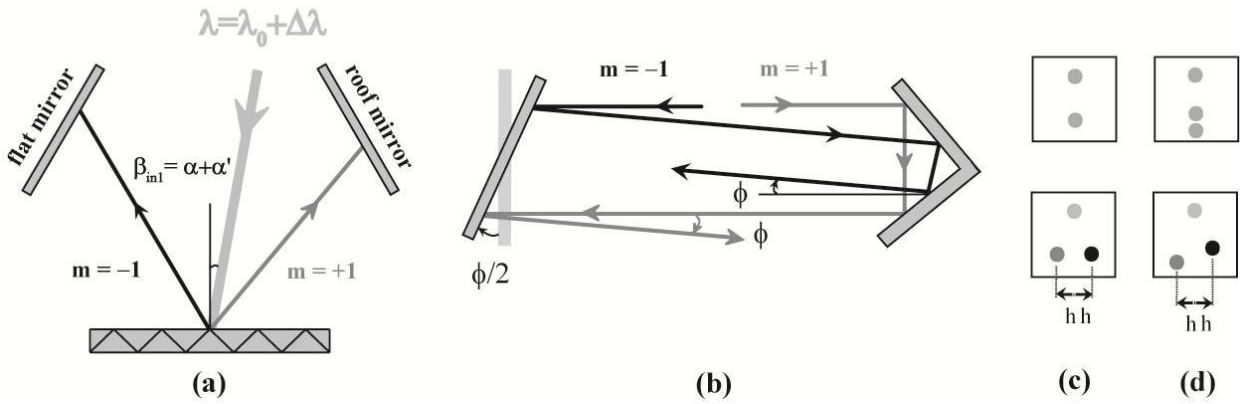

Figure 5. (a) A downward facing view toward the interference plane. (b) A horizontal view of the optical paths with respect to the roof mirror. It can be seen that the m=+1 order (black) is incident on the roof mirror first and exits downward, while the m= –1 order (dark gray) is incident on the flat mirror first and exits upward. In (c) and (d), the upper frames show the location of the beams on the grating for the heterodyne wavelength with $\beta_{in1}=0$, while bottom squares are for $\lambda=\lambda_0+\Delta\lambda$ coming in with $\beta_{in1}=\alpha+\alpha'$. (c) Shows the spots on the grating if $\phi=0$. (d) Shows the spots on the grating if $\phi\neq0$. For clarity, the angles and the distances are exaggerated and the colors are preserved.

Use of a roof mirror provides a method for resolving the aliasing degeneracy in $\pm\Delta\lambda$. An alignment modification of the roof mirror configuration allows separation of features with the same *absolute* $\Delta\lambda$, but opposite in sign with respect to λ_o by introducing a y-axis frequency into the pattern. If we introduce an internal tilt $\phi/2$ in the flat mirror perpendicular to the grating's diffraction plane, the roof mirror reflection will introduce a $+\phi$ incline to the beam that strikes the flat mirror first and $-\phi$ incline to the beam that strikes the roof mirror first.

This modification will change the β_{out2} and therefore the generated fringe intensity pattern. The outgoing beam angles in this configuration can be shown to be:

$$\beta_{out\,2} = \sin^{-1}\left\{\frac{\sin\,\beta_0 + mG\,\Delta\lambda}{\cos\,(\alpha'+\phi)} - \sin(\beta_0 - \Delta\bar{\beta})\right\}, \tag{9}$$

and the spatial fringe frequencies is given by:

$$\begin{aligned} f_x &= \sigma \sin\beta_{out\,2}\{\cos(\alpha'+\phi) + \cos(\alpha'-\phi)\}, \\ f_y &= \sigma\{\sin(\alpha'+\phi) - \sin(\alpha'-\phi)\}, \\ f_z &= \sigma\cos\beta_{out\,2}\{\cos(\alpha'+\phi) - \cos(\alpha'-\phi)\}. \end{aligned} \tag{10}$$

At the fringe localization plane, the fringe pattern has special intensity I(x,y,z) distribution given by:

$$I(x) = \int_0^\infty S(\sigma)\{1 + \cos 2\pi(f_x x + f_y y + f_z z)\}d\sigma. \tag{11}$$

The z frequency is the smallest of the three axes, such that the fringe contrast slowly varies in this direction. The f_y rotation breaks the aliasing degeneracy in the sense that wavelengths greater than λ_o and less than λ_o appear rotated in opposite directions. A two dimensional Fourier transform of $I(x,y,z_0)$ recovers the input power spectrum with zero spatial frequency corresponding to $\sigma=\sigma_o$. However, the rotation direction places the output frequencies on the correctly in wavelength with respect to the heterodyne wavelength. It is clear by eliminating the rotation in the flat mirror (perpendicular to the interference plane), the 3 dimensional fringe pattern breaks into a series of vertical fringes of frequency f_x and that f_y and f_z disappear.

2.3 Resolution and Bandpass

The resolving power of a SHS system is defined as the smallest $\Delta\lambda_R$ that accumulates to a one-fringe change in frequency over the *entire* fringe localization plane. This conceptually merges the width of the incoming beam with the width of localization plane, which is really an interferometric representation of the grating. Since the theoretical resolving power of a grating is directly related to the number of grooves illuminated, a reduction in the width of the plane automatically reduces the resolving power. If W is the width of the beam on the grating, and N is the total number of fringes on the fringe localization plane, we will have $N= f\times W$. Since f_z is much smaller than f_x and f_y, in general, we can find the resolving power with the condition of one fringe over the entire fringe localization plane by the smallest values from $f_x=1$ and $f_y=1$. The resolving power in small angle approximation for $\beta_{in1}=0$ ($\alpha=\alpha'=0$) is

$$R = \frac{\sigma_0}{|\sigma_0 - \sigma|} = 4mGW\,. \tag{12}$$

It can be seen that the resolution becomes extremely high as the illuminated area of the grating size increases. The implications of this are that for a given number of resolvable fringes the bandpass is tied directly to the resolution, since each frequency corresponds to nearly the same $\Delta\lambda$. This bandpass limitation becomes more severe as one move into the UV where both λ_o and $\Delta\lambda$ become smaller. As we will show later, the spectral coverage is related to 1/R, therefore a major difficulty with SHS systems is in keeping the resolution low enough to sample a useful bandpass.

For the incoming beam, the mechanical limits to the bandpass come from the efficiency profile of the grating and the size of the mirrors. As a practical matter, neither of these are significant issues because a very large bandpass is usually covered by small changes in either quantity for a given heterodyne wavelength. The useful bandpass of SHS is far more limited by the number and size of pixels at the detector. The spatial frequency of fringes is determined by the offset of a given wavenumber from the heterodyne wavelength, with the spacing between frequencies determined by the resolving power and λ_0. The practical limit of the bandpass is given by the Nyquist limit of the detector. The bandpass can be determined by $\pm\Delta\lambda_B$ around λ_0, so the value of the bandpass or the wavelength range will be from $\lambda_0-\Delta\lambda_B$ to $\lambda_0+\Delta\lambda_B$. $\Delta\lambda_B$ for normal incoming light ($\alpha=\alpha'=0$) in small angle approximation is given by

$$\Delta\lambda_B = \frac{\lambda_0}{\frac{Rk}{N} - 1} \tag{13}$$

where R is the resolving power, k is the minimum number of pixels required to resolve one fringe (for the Nyquist limit: k=2), and N is the total number of pixels along the detector. Typical single-tune configurations have useful bandpasses of $2|\Delta\lambda_B|<10$nm. Light at other wavelengths still interferes and reaches the detector, but their frequencies are recorded as unresolved noise. It should be noted that this represents a purely theoretical limit. Distortions in the optics, the modulation transfer function of the detector pixels, and the match of pattern to the fixed pixel array all combine to produce a significantly smaller bandpass in practice.

2.4 Tuning feature

A straightforward method for increasing the bandpass of a SHS is to change the heterodyne wavelength of the instrument by rotating one or both of the mirrors around the axis normal to the grating diffraction plane. Provided the secondary capabilities exist for maintaining precision control of the rotation and the ability to adjust to changes in the fringe localization plane, this allows the use of a single SHS instrument for studies of multiple bands of interest. In this case, the only limitations come from the size of the mirrors, the wavelength dependent efficiency changes in the grating, and the properties of the detector.

In section 2.1, we note that if $\beta_{out1}=\beta_0+\Delta\bar{\beta}$ then $\beta_{in2}=\beta_0-\Delta\bar{\beta}$. Consequently, if we could change the β_{out1} angle of the beam as by $2\Delta\bar{\beta}$, by rotating each mirror by $\Delta\bar{\beta}/2$, the beam will be incident on the grating for second time at $\beta_{out2}=\beta_0+(2\Delta\bar{\beta})-\Delta\bar{\beta}=\beta_0+\Delta\bar{\beta}$. Hence, $\lambda=\lambda_0+\Delta\lambda$ would be the new heterodyne wavelength. When the SHS is tuned to λ_0, the angle between the two mirrors will be:

$$\delta = \frac{\pi}{2} - \beta_0 \, . \tag{14}$$

If we tune the SHS to $\lambda=\lambda_0+\Delta\lambda$, β_0 will change to $\beta_0'=\beta_0+\Delta\bar{\beta}$ and therefore the new angle between the two mirrors will be:

$$\delta' = \frac{\pi}{2} - (\beta_0 - \Delta\bar{\beta}). \tag{15}$$

Rotating one mirror will affect both arms and can result in the same change in heterodyne wavelength. For a total effect of $2\Delta\bar{\beta}$, we need to rotate one mirror by

$$\theta = \Delta\bar{\beta} \, . \tag{16}$$

Another way to extend the bandpass of a SHS is to change the grating's groove density. It is possible to use a grating wheel containing gratings with different groove densities, and use them for different heterodyne wavelengths with the same rotation angles in the pilot mirrors. Conserving the geometry of the SHS, the relationship between the original heterodyne wavelength and the new heterodyne wavelength is

$$\lambda_{01} G_1 = \lambda_{02} G_2 \quad (17)$$

The primary advantage of this method is that changing gratings allows a single series of tuning angles to sample more than one range of wavelengths. For a broadly tunable design such as the one discussed below in section 3, this allows the mechanical structures and optics to be greatly reduced in size and in their range of motion.

3. SECOND GENERATION ALL REFLECTIVE TUNABLE SHS

The first generation anti-aliased all-reflective tunable SHS prototype was developed by Dawson and Harris [14] at the University of Washington, Department of Earth and Space Sciences. This instrument was successfully tested at the Kitt Peak McMath-Pierce solar observatory where it was used to observe Venus and Jupiter. The results from the first generation suggested some problems in the instrument's design that we are addressing in the second generation as it comes in the below.

The second generation all reflection tunable SHS is being built at Applied Science Department, University of California Davis with the support from the NASA Planetary Instrument Design and Development Program (PIDDP). We are currently working with an optical bench prototype. This prototype addresses the main known problems in the first generation and will be used to optimize the opto-mechanical design for a field instrument that will be constructed for a field testing as part of the large campaign to study comet 103P/Hartley 2 in late 2010. In addition to the quality of the instrument-target match, the large number of near-simultaneous observations with other instruments will provide excellent opportunity to compare and verify the performance of the new instrument. . The target spectral range for the instrument is 300-700 nm. In addition to addressing some performance issues with the optical components and their mounts, the primary areas of modification involve the number and characteristics of the gratings, the output optical system, and the tuning mechanism.

The first generation design used a single grating for the entire tuning bandpass. The problem with this design is two-fold. First is the consistency of the grating efficiency over such a large spectral range. The best efficiency, for any grating, is rarely obtained over a wavelength range larger than 400 nm. This made it technically impractical to use one grating for a very large bandpass. However, even if the grating were to allow a large bandpass (e.g., a factor of 2 or greater in wavelength) at high efficiency, the size of the mirrors necessary to accommodate the resulting large angular range makes the design cumbersome and more prone to optical distortions. In addition, as noted in section 2.1, the location of the fringe localization plane changes over a large tuning range with a single grating and a large span of dispersion angles. To get around these limitations in our design, we are using a grating wheel to exchange the grating's groove density for tuning to the blue and red portions of the target wavelength scale. Using the equation (17), the same range of angles will sample two wavelength bands, conserving the geometry of the system. Differences in the resolving power can be compensated by increasing the illuminated area of the grating, which has the side benefit of increasing the étendue for half the spectral range.

The reimaging optics in the first generation SHS were on axis achromatic spherical lenses that suffered from significant aberrations and variability in the magnification of fringe localization plane on the detector. The new design moves to a fully all-reflective, aberration corrected configuration in the output optics. For the current design, we will use the off axis all reflective Offner design that was introduced by Lawler et al. [16]. The Offner configuration can be constructed with a fixed fringe localization plane magnification and corrects for the primary aberrations that was dominated in the first SHS version.

The tuning feature in the first generation required the symmetric rotation of both mirrors, which compounded any inaccuracy in both rotation stages and the mirror mounts. It also required precise alignment of the axes of both stages with the center of mirrors. In addition, the design required same large formats for both the roof mirror and the flat mirror. As it was discussed in section 2.4, it is possible to tune the SHS to another wavelength by rotating only one mirror. In current design, we are planning to rotate only the roof mirror and have the flat mirror in a fixed position. The main

advantage of this design, besides eliminating one rotation stage and saving its space and weight, is that we can use a much smaller, and therefore more stable, roof mirror.

Figure 6 and 7 show sample results from Hg and Na test lamps. These results are generated as a test run and more efforts are required before concluding about the final performance of this instrument. They are being provided here to show the tuning feature of the instrument and the effect of the cross tilt in the flat mirror for resolving the aliasing problem.

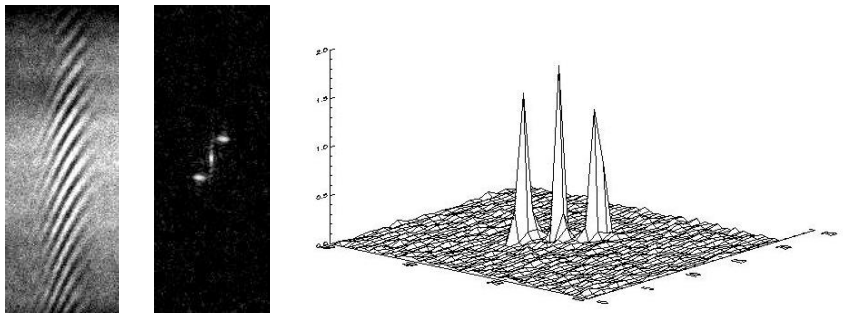

(a) **(b)** **(c)**

Figure 6. (a) A sample fringe pattern for Hg lamp, λ= 5461Å, with cross tilt in the flat mirror. The heterodyne wavelength in this setup is λ_0= 5463Å. The narrowness of the interference pattern comes from opening the aperture beyond the maximum FOV. (b) Above view from the 3 dimensional power spectrum. (c) The 3D power spectrum.

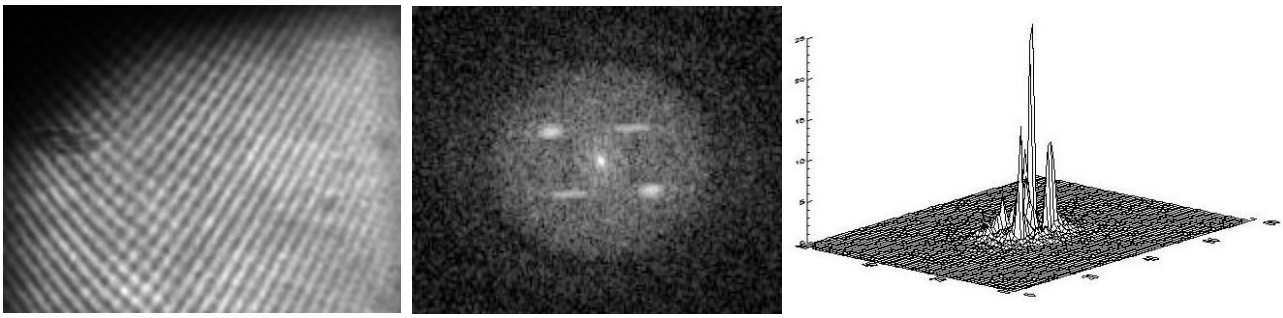

(a) **(b)** **(c)**

Figure 7. (a) A sample fringe pattern for Na lamp D lines: λ_1= 5895.9Å and λ_2= 5889.9Å.The heterodyne wavelength in this setup is λ_0= 5892Å. The cross tilt in the flat mirror, rotates the separating two Sodium D lines in opposite directions. (b) Above view from the 3 dimensional power spectrum. It is clear how the spectrum lines are separated in the anti aliasing design. (c) The 3D power spectrum.

4. ACKNOWLEDGMENT

This research was supported by NASA grant NNX07AU10G to the University of California, Davis. Also, we gratefully acknowledge the assistance provided by Yan Bétrémieux.

5. REFERENCES

[1] Harlander, J., Reynolds, R. J., and Roesler, F. L., “Spatial Heterodyne Spectroscopy for the Exploration of Diffuse Interstellar Emission Lines at Far Ultraviolet Wavelengths”, Astrophys. J. 396, 730-740 (1992).

[2] Harlander, J., Reynolds, R. J., and Roesler, F. L., “Spatial Heterodyne Spectroscopy for the Exploration of Diffuse Interstellar Emission Lines at Far Ultraviolet Wavelengths”, Astrophys. J. 396, 730-740 (1992).

[3] Christensen, P. R., Mehall, G. L., et al., "Miniature thermal emission spectrometer for the Mars Exploration Rover", Acta Astronautica, 59 (8-11): 990–999 (2003).

[4] Kruger, R. A., Anderson, L. W., and Roesler, F. L., "New Fourier Transform All-Reflection Interferometer," Appl. Opt. 12, 533-540 (1973).

[5] Sheinis, A. I., Mierkiewicz, E., et al., “A spatial heterodyne spectrometer for diffuse H-α spectroscopy”, Proc. SPIE, Vol. 7014, pp. 70140I-70140I-12 (2008).

[6] Englert, C. R., Stevens, M. H., et al., “Inter-seasonal observations of Mesospheric Hydroxyl by SHIMMER”, American Geophysical Union, Fall Meeting (2009).

[7] Chakrabarti, S., Cotton, C., et al., “Self-compensating, all-reflection interferometer”, Applied Optics, Vol. 33, Issue 13, pp. 2596-2607 (1994).

[8] Harris, W. M., Dawson, O. R., “A broadband spatial hetrodyne spectrometer for high resolution studies of faint extended emission sources”, presented at the Joint Fourier Transform Spectroscopy and Hyperspectral Imaging and Sounding of the Environment Meeting of the Optical Society of America, Santa Fe, New Mexico, 11–15, February (2007).

[9] Harlander, J. M., “Spatial heterodyne spectroscopy : interferometric performance at any wavelength without scanning”, Thesis (Ph.D.)—University of Wisconsin—Madison (1991).

[10] Connes, P., "Spectrometre interferentiel a selection par l'amplitude de modulation," Le Journal de Physique et le Radium, 19 , p. 215 (1958).

[11] Dohi, T., and Suzuki, T., “Attainment of High Resolution Holographic Fourier Transform Spectroscopy”, Applied Optics 10, 1137-1140 (1971).

[12] Roesler, F. L., and Harlander, J., “Spatial Heterodyne Spectroscopy: Interferometric performance at any wavelength without scanning”, Proc. SPIE, Vol. 1318, 234 (1990).

[13] Harlander, J. M., and Roesler, F. L., “Spatial heterodyne spectroscopy. A novel interferometric technique for ground-based and space astronomy,” Proc. SPIE 1235, 622–633 (1990).

[14] Dawson, O. R., and Harris, W. M., “Tunable, all-reflective spatial heterodyne spectrometer for broadband spectral line studies in the visible and near-ultraviolet”, Applied Optics 48, 4227-4238 (2009).

[15] Harris, W. M., F. Roesler, et al. “Applications of reflective spatial heterodyne spectroscopy to UV exploration in the solar system”, Proc. SPIE, Vol. 5488, 886 (2004).

[16] Lawler, J. E., Labby, Z., Harlander, J. M., and Roesler, F. L., “Broadband, high-resolution spatial heterodyne spectrometer”, Applied Optics 47, 6371-6384 (2008).